Profiling the Phospho-status of the BK$_{Ca}$ Channel α Subunit in Rat Brain Reveals Unexpected Patterns and Complexity*⑤

Jiusheng Yan‡§, Jesper V. Olsen¶, Kang-Sik Park‡, Weiyan Li§, Wolfgang Bildl‖, Uwe Schulte, Richard W. Aldrich§, Bernd Fakler‖‡‡, and James S. Trimmer‡§§¶¶**

Molecular diversity of ion channel structure and function underlies variability in electrical signaling in nerve, muscle, and non-excitable cells. Protein phosphorylation and alternative splicing of pre-mRNA are two important mechanisms to generate structural and functional diversity of ion channels. However, systematic mass spectrometric analyses of *in vivo* phosphorylation and splice variants of ion channels in native tissues are largely lacking. Mammalian large-conductance calcium-activated potassium (BK$_{Ca}$) channels are tetramers of α subunits (BKα) either alone or together with β subunits, exhibit exceptionally large single channel conductance, and are dually activated by membrane depolarization and intracellular Ca^{2+}. The cytoplasmic C terminus of BKα is subjected to extensive pre-mRNA splicing and, as predicted by several algorithms, offers numerous phospho-acceptor amino acids. Here we use nanoflow liquid chromatography tandem mass spectrometry on BK$_{Ca}$ channels affinity-purified from rat brain to analyze *in vivo* BKα phosphorylation and splicing. We found 7 splice variations and identified as many as 30 Ser/Thr *in vivo* phosphorylation sites; most of which were not predicted by commonly used algorithms. Of the identified phosphosites 23 are located in the C terminus, four were found on splice insertions. Electrophysiological analyses of phospho- and dephosphomimetic mutants transiently expressed in HEK-293 cells suggest that phosphorylation of BKα differentially modulates the voltage- and Ca^{2+}-dependence of channel activation. These results demonstrate that the pore-forming subunit of BK$_{Ca}$ channels is extensively phosphorylated in the mammalian brain providing a molecular basis for the regulation of firing pattern and excitability through dynamic modification of BKα structure and function. *Molecular & Cellular Proteomics 7:2188–2198, 2008.*

Ion channels are membrane proteins responsible for electrical signaling in nerve, muscle, and non-excitable cells (1). The diversity in electrical properties of different cell types, or of the same cell type at different developmental stages or physiological conditions, is defined not only by expression and subunit composition of distinct ion channels, but also by posttranscriptional and posttranslational modifications of their component subunits (1, 2). Alternative splicing of pre-mRNA to yield changes in primary structure and protein phosphorylation to alter folding and charge are fundamentally important mechanisms to generate structural and functional diversity of ion channel proteins (3–8). To date, however, systematic investigations of *in vivo* phosphorylation and splicing by direct analyses of ion channel proteins are largely lacking (7).

Mammalian BK$_{Ca}$ (large-conductance calcium-activated potassium, also termed K$_{Ca}$1.1, Maxi-K, or Slo1)[1] channels are unique potassium-selective channels that are dually activated by two independent physiological signals: intracellular Ca^{2+} concentration and transmembrane voltage (9–12); thereby playing a powerful integrative role in the regulation of electrical excitability through coupling of calcium signaling and cellular excitability. In mammalian central neurons, BK$_{Ca}$ channels underlie the repolarization and fast after-hyperpolarization of action potentials (13, 14), shape dendritic Ca^{2+} spikes (15), and control neurotransmitter release at presynaptic terminals (16, 17). BK$_{Ca}$ channels also play key roles in other diverse physiological processes such as contractile tone of various types of smooth muscle cells, frequency tuning of auditory hair cells, hormone secretion, and innate immunity (9–11).

BK$_{Ca}$ channels are robustly expressed in central neurons throughout most regions of the mammalian brain (18). Unlike

From the ‡Department of Neurobiology, Physiology and Behavior, College of Biological Sciences, University of California, Davis, California 95616, §Section of Neurobiology, School of Biological Sciences, University of Texas, Austin, Texas 78712, ¶Department of Proteomics and Signal Transduction, Max Planck Institute for Biochemistry, D-82152 Martinsried, Germany, ‖Institute of Physiology, University of Freiburg, Hermann-Herder-Strasse 7, 79104 Freiburg, Germany, **Logopharm GmbH, Hermann-Herder-Strasse 7, 79104 Freiburg, Germany, §§Department of Physiology and Membrane Biology, School of Medicine, University of California, Davis, California 95616

[1] The abbreviations used are: BK$_{Ca}$, large conductance calcium- and voltage-activated potassium channel; BKα, BK channel α subunit; WT, wild type; LC-MS/MS, liquid chromatography tandem mass spectrometry; RCK, regulating conductance of K$^+$; HEDTA, *N*-(2-hydroxyethyl)ethylenediaminetriacetic acid; PKA, protein kinase A.

many mammalian potassium channels, a single gene (*Slo1*, *KCNMA1*) encodes all BK$_{Ca}$ channel α subunits (BKα). However, native BK$_{Ca}$ channels display a broad range of functional properties that differ between different cells (9, 10), at different stages of development (19, 20), and under different physiological conditions (21). In addition to assembly with tissue-specific auxiliary β subunits (β1-β4), diversity in the physiological properties of BK$_{Ca}$ channels can be generated by extensive pre-mRNA splicing and phosphorylation of BKα.

BK$_{Ca}$ channels are tetramers of the pore-forming, voltage-, and Ca^{2+}-sensing BKα either alone or in association with regulatory β subunits. BKαs are 125–140 kDa polypeptides containing seven transmembrane segments (S0–S6), a short extracellular N-terminal domain, and a large cytoplasmic C terminus (22) (Fig. 1). This C-terminal domain comprises >70% of the total protein and contains four hydrophobic segments (S7–S10) and sequences similar to RCK (Regulating Conductance of K^{+}) domains (23–25), and a string of Asp residues known as the "Ca^{2+} bowl" (26).

BKα contains ~200 serine and threonine residues that can be potentially phosphorylated by cellular protein kinases (supplemental material). Modulation of native and cloned BK$_{Ca}$ channels by protein kinases is well established (27–30). In smooth muscle, protein kinases PKA, protein kinase G, and protein kinase C play an important role in BK channel-mediated regulation of contractility (reviewed in Ref. 8). In central neurons, both enhancement and inhibition of BK$_{Ca}$ channel activity by PKA have been observed (28, 31, 32). However evidence for direct phosphorylation and a systematic analysis of BK$_{Ca}$ channel phosphorylation in native tissue are lacking. Alternative splicing has been extensively studied at the mRNA level in different species and tissues, and more than 20 BKα splice variants have been identified (2, 33, 34). However, no information on expression of the polypeptide products of these alternatively spliced mRNAs is yet available at the protein level.

To help understand the molecular structure and diversity of BK$_{Ca}$ channels in the central nervous system, we have immunopurified BKα from rat brain and taken an unbiased approach using nanoflow tandem mass spectrometry (nano-LC MS/MS) to systematically analyze their *in vivo* phosphorylation sites and splice variants. We have identified extensive *in vivo* phosphorylation of native BKα and examined the functional consequence of phosphorylation at a number of identified sites by electrophysiological analyses of phospho- and dephosphomimetic BKα mutants transiently expressed in HEK-293 cells.

EXPERIMENTAL PROCEDURES

Affinity Purification of BK$_{Ca}$ Channels from Rat Brain—Two different sets of affinity purifications of BK$_{Ca}$ channels were used in this study. One set employed monoclonal antibody-based immunopurification from rat brain membranes prepared from freshly isolated adult whole rat brains as described (35) and solubilized by 1% Triton X-100 or 1% dodecyl-maltoside. BKα was affinity-purified using the monoclonal antibody L6/60 (termed *anti-BKα_1*) (36, 37) immobilized on protein G agarose beads. L6/60 binds within amino acid residues 729–930 of mouse BKα (UniProt/Swiss Prot accession number Q08460). Phosphatase inhibitors (10 mM NaF, 1 mM sodium orthovanadate, 5 mM sodium pyrophosphate) and protease inhibitors were used throughout the procedure. The other set of affinity purifications used two polyclonal antibodies with plasma membrane-enriched protein fractions prepared from adult rat brains as described previously (38, 39). Almost complete solubilization (>95% as judged from densitometric estimates of Western-probed solubilisate *versus* pellet) was achieved with 1–1.25 ml of ComplexioLyte 48 (including protease inhibitors; Logopharm GmbH, Freiburg, Germany) per mg membrane protein. 1.5 ml of solubilisate was incubated with 20 μg immobilized rabbit polyclonal antibodies raised either against amino acid residues 1184–1203 (termed anti-BKα_2, gift from Dr. Hans-Guenther Knaus, University of Innsbruck) or 1184–1200 (termed *anti-BKα_3*, Alomone Labs, Jerusalem, Israel) of the mouse BKα (UniProt accession number Q08460). Bound proteins were eluted with Laemmli buffer (dithiothreitol added after elution). Aliquots from each step were analyzed on Western blots with equivalent fractions (as in Fig. 1*B*, lanes *1*, *2* of each affinity purification and supplemental Fig. S4) to ensure quantitative purification and recovery of intact BKα protein.

In-gel Digestion and Enrichment of Phosphopeptides—Affinity-purified proteins were separated by SDS-PAGE and either silver-stained (in the absence of cross-linkers) or visualized with Coomassie G-250. Bands containing BKα (as validated by Western analysis) as well as complete lanes were separately excised and washed thoroughly with 50% acetonitrile in 25 mM ammonium bicarbonate. In-gel digestion was carried out essentially as described by (40). After reduction and alkylation of Cys residues using dithiothreitol and iodoacetamide, gel pieces were washed, dehydrated, and subsequently swollen with ammonium bicarbonate buffer containing 10 ng/μl trypsin (Promega, Madison, WI) and incubated for ~16 h at 37 °C. Digested peptide mixtures were extracted, dried in a speed vacuum concentrator, and finally redissolved in 0.2–0.5% formic acid (protein samples obtained from *anti-BKα_1* eluates) or trifluoroacetic acid (protein samples obtained from *anti-BKα_2* and *anti-BKα_3* eluates).

The peptide mixtures were either directly used for MS analyses or further processed to enrich the phosphopeptides. Phosphopeptide enrichment and tandem mass spectrometric analysis were performed essentially as described previously (41, 42) with a few modifications. Briefly, a slurry of titanium dioxide beads precoated with 2,5-dihydrobenzoic acid was prepared by mixing 10 μg of titansphere TiO$_2$ beads (GL Sciences) with 20 μl of 30 mg/ml 2,5-dihydrobenzoic acid (Fluka) in 80% acetonitrile. 5 μl of this 2,5-dihydrobenzoic acid/TiO$_2$ slurry was added to the acidified peptide mixtures, extracted from in-gel digests. The peptide mixtures were shaken for 30 min at 1000 rpm at 4 °C, and then spun down in a microcentrifuge. The pelleted TiO$_2$ beads were washed twice with 30% acetonitrile in 3% trifluoroacetic acid, and peptides were eluted with 15% NH$_4$OH in 40% acetonitrile (pH > 10.5). Finally, the eluates were dried in a speed vacuum concentrator for 20 min at 45 °C and reconstituted in 8 μl of 2% acetonitrile in 0.1% trifluoroacetic acid to prepare them for LC-MS.

Mass Spectrometry, Data Processing, and Analysis—BKα affinity-purified with the monoclonal antibody *anti-BKα_1* was analyzed with an LTQ ion trap or LTQ-FT hybrid mass spectrometer (Thermo-Fisher, San Jose, CA) connected to a Waters UltraPerformance LC system (Waters, Milford, MA). Peptide samples were concentrated on a Waters Symmetry C18 280 μm × 20 mm nanoAcquity trap column at a loading flow rate of 15 μl/min. Peptides were then eluted from the trap and separated by a Waters 100 μm × 100 mm UltraPerformance LC column using a 90 min gradient of 2–80% buffer B (buffer A, 0.1% formic acid, buffer B, 95% acetonitrile, 0.1% formic acid), and sprayed into an LTQ or LTQ-FT ion trap mass spectrometer through a nanoelectrospray source. The MS survey scan was acquired using

the LTQ or Fourier transform ion cyclotron resonance mass analyzer and then the top four ions in each survey scan were subjected to automatic low energy collision-induced dissociation for MS/MS scans.

MS/MS spectra were extracted using the program Extract_msn v.4.0 of the Bioworks software v.3.3 (Thermo Finnigan) with default parameters and interpreted with Mascot v.2.2 (Matrix Science, London, UK) and Sequest/Bioworks v.3.3 search engines by searching against UniProt/Swiss-Prot database (release 50.8, subset Rodents, 18284 protein entries) supplemented with all known and artificially spliced variants of rat BKα (rSlo), based on the rat genomic sequence and known splicing variants from mRNA or expressed sequence tag sequence of other mammalian species. Database searches were performed with a peptide mass tolerance of 2 Da (LTQ) or 20 ppm (LTQ-FT), MS/MS tolerance of 0.4 Da, and strict tryptic specificity (cleavage after lysine and arginine) allowing one missed cleavage site; carbamidomethylation of Cys was set as fixed modification, whereas oxidation (Met), *N*-acetylation, *N*-pyroglutamine formation, and phosphorylation (Ser, Thr, Tyr) were considered as variable modifications. Peptide ions with a Mascot ion score of <20 were manually checked for validation. For database search with Sequest/Bioworks, peptide sequences from the search result were filtered out with criteria of correlation value (Xcorr) >1.5, 2.0, and 3.0 for singly, doubly, and triply charged peptide ions, respectively, and ΔCn (difference in correlation with the next higher Xcorr) >0.08. Each MS/MS spectrum exhibiting possible phosphorylation was manually checked and validated based on the existence of a 98 Da mass loss (H$_3$PO$_4$; phosphopeptide-specific collision-induced dissociation neutral loss) for both precursor and fragmented ions.

The peptide mixtures from BKα affinity-purified with the polyclonal antibodies *anti-BKα_2* and *anti-BKα_3* were separated by online high pressure liquid chromatography and directly electrosprayed into an LTQ-Orbitrap hybrid mass spectrometer as described (41). The instrument was operated in data-dependent mode to automatically switch between full scan MS and MS/MS acquisition. All full scans were acquired with a resolution of 60,000 at m/z = 400 by the Orbitrap detector system using automatic internal lock-mass recalibration in real-time (43). From each full scan up to five peptide ions with charge states ≥2 were selected for fragmentation by multi-stage activation (multistage activation or pseudo MS^3) (44). All fragment ion spectra were recorded with the LTQ detectors.

MS/MS peak lists were extracted from the raw MS files by in-house written software Raw2msm v.1.10 (43) using default parameters (intensity-weighing the parent ion m/z over the LC elution profile and keeping top 6 most intense fragment ions per 100 m/z units), and searched by Mascot v.2.2 against a concatenated forward (target) and reversed (decoy) version of the IPI rat database v.3.25 supplemented with standard observed contaminants such as porcine trypsin and human keratins (total number of protein sequences: 82886). Carbamidomethylation of cysteine residues was set as a fixed modification, whereas oxidation (Met), *N*-pyroglutamine formation, and phosphorylation (Ser, Thr, Tyr) were considered as variable modifications. Full tryptic specificity (cleavage after lysine and arginine) was required and up to three missed cleavages were allowed. The initial mass tolerance in MS mode was set to 5 ppm and MS/MS mass tolerance was 0.5 Da. The resulting Mascot html-output file was linked to the raw MS files and loaded into the MSQuant software only accepting the highest-scoring peptide sequence for each MS/MS spectrum and requiring a minimum Mascot score of at least 10. To minimize the false discovery rate all peptide identifications were filtered by thresholds on peptide length, mass error, and Mascot score. We fixed the thresholds and accepted peptides based on the criteria that the number of forward hits were at least 200-fold higher than the number of reversed hits, which gives an estimated false discovery rate of less than 1% ($p <$ 0.01). To pinpoint the actual phosphorylated amino acid residue within the identified phosphopeptides in an unbiased manner, we calculated the localization probabilities of all Ser and Thr phosphorylation sites using the post-translational modification score algorithm as described (41).
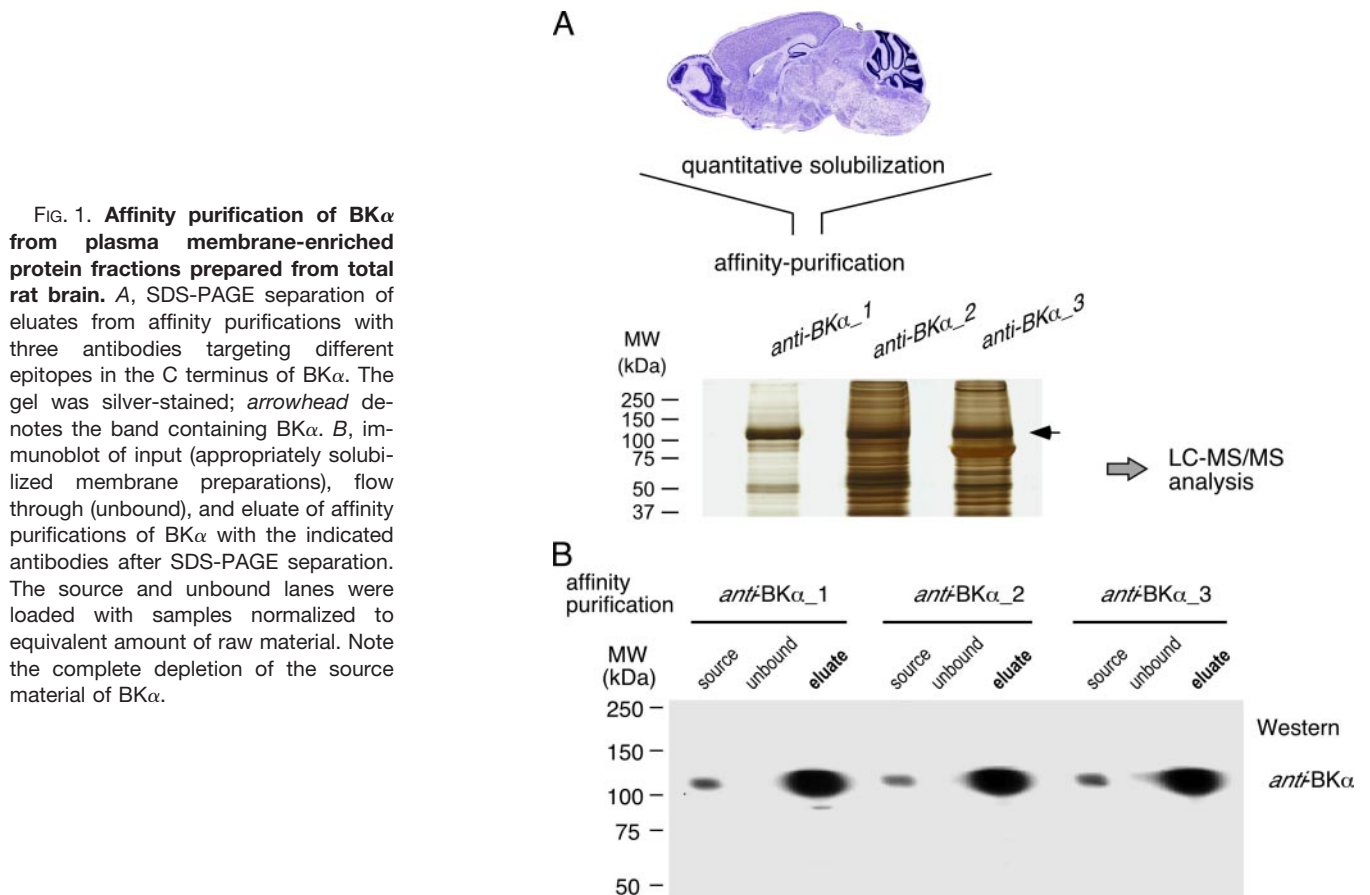
Site-directed Mutagenesis and Heterologous Expression in Culture Cells—Phosphorylation site mutants were constructed with the recombinant cDNA plasmid, HF1-hSlo (45) encoding c-Myc-tagged human BKα (EMBL-Bank accession number AAB65837). HEK-293 cells were cultured in Dulbecco's modified Eagle's medium (Invitrogen) with 10% fetal bovine serum (Hyclone, Logan, UT), 50 units/ml penicillin, 50 mg/ml streptomycin, and GlutaMAX^{TM} (Invitrogen). Cells were maintained in a humidified atmosphere of 5% CO$_2$ at 37 °C and transiently transfected with HF1-hSlo1 plasmid together with pEGFP-C1 using Lipofectamine (Invitrogen). All cells were used within 16–72 h after transfection for electrophysiological assays.

Electrophysiological Recordings and Data Analysis—All recordings were performed at room temperature in the inside-out patch-clamp configuration. Data were acquired with an Axopatch 200A patch-clamp amplifier (Axon Instruments, Inc.) in resistive feedback mode and were low pass filtered at 10 kHz with its 4-pole Bessel filter. An ITC-16 hardware interface (Instrutech) and Pulse acquisition software (HEKA Elektronik) were used to sample the records at 20-μs intervals. Capacitive transients and leak currents were subtracted by a P/5 protocol at holding potentials of −120 mV or −150 mV (for recordings with 103 μM intracellular Ca^{2+}). Four to eight consecutive current series were averaged to increase the signal to noise ratio. Normalized conductance-voltage relationships were fitted with single Boltzmann functions: $G/G_{max} = 1/(1 + e^{(V1/2 - Vm)*zF/RT})$, with $V_{1/2}$ the half-maximal voltage of activation, and z the equivalent gating charge.

Pipette (external) solution contained (in mM): 140 KMeSO$_3$, 20 HEPES, 2 KCl, and 2 MgCl$_2$, pH 7.20. Bath (internal) solution: 136 KMeSO$_3$, 20 HEPES, 6 KCl, pH 7.20. Internal solutions with defined concentrations of free Ca^{2+} ([Ca^{2+}]$_i$) were obtained by adding Ca^{2+} chelators EGTA, HEDTA, or nitrilotriacetic acid and CaCl$_2$ to the bath solution as calculated with the WEBMAXC v2.22; the final [Ca^{2+}]$_i$ was measured with a Ca^{2+}-sensitive electrode (Orion Research, Inc.). To chelate contaminant Ba^{2+}, 40 μM fresh (+)-18-crown-6-tetracarboxylic acid (18C6TA) was added to the internal solution just before recording. Inside-out patches were continuously perfused with internal solution using a sewer pipe flow system (DAD-12; Adams and List Assoc., Ltd.); computer-controlled switches allowed for complete solution exchange at excised patches in <1 s.

RESULTS

MS Analyses of Rat Brain BKα: Primary Sequence Coverage and Splice Variations—Two independent proteomic analyses of BKα affinity-purified from membrane preparations of total rat brain form the basis of this study. One set of analyses used BKα immunopurified with a BKα-specific mouse monoclonal antibody binding near the S9 region (*anti-BKα_1*) (37), the other used BKα immunopurified with two different rabbit polyclonal antibodies (*anti-BKα_2*, *anti-BKα_3*) recognizing short peptide sequences within the C-terminal tail region (38). All three antibodies were highly effective in affinity purifications fully depleting the source material of BKα (Fig. 1). After separation on SDS gels, BKα proteins were in-gel digested with trypsin, and the resultant tryptic peptides were analyzed by nanoflow liquid chromatography tandem MS (nano-LC MS/MS) using a linear ion trap or high resolution hybrid mass spectrometers (LTQ, LTQ-FT, or LTQ-Orbitrap).

FIG. 1. **Affinity purification of BKα from plasma membrane-enriched protein fractions prepared from total rat brain.** *A*, SDS-PAGE separation of eluates from affinity purifications with three antibodies targeting different epitopes in the C terminus of BKα. The gel was silver-stained; *arrowhead* denotes the band containing BKα. *B*, immunoblot of input (appropriately solubilized membrane preparations), flow through (unbound), and eluate of affinity purifications of BKα with the indicated antibodies after SDS-PAGE separation. The source and unbound lanes were loaded with samples normalized to equivalent amount of raw material. Note the complete depletion of the source material of BKα.

Based on the high yield of our affinity purifications, mass spectrometry retrieved ≥60 BKα-specific peptides, which is almost the complete set obtainable under our experimental conditions. Together, these peptide fragments cover ~70% of the BKα amino acid sequence as encoded by the 27 exons considered constitutive (34) (Fig. 2*A*). The non-covered regions are hydrophobic segments of the transmembrane core, and a short segment of the cytoplasmic C terminus for which no peptides could be detected because of the unfavorable mass of the resultant tryptic peptides (molecular weight of detectable peptide fragments between 740 and 3000). In addition, MS analysis retrieved a number of peptides that correspond to entries in a custom database of BKα splice variants, and demonstrate expression of these isoforms of BKα in the rat brain (supplemental Table S2). Fig. 2*B* illustrates the amino acid sequences of the peptide fragments that define these variations from the constitutive BKα primary sequence. Together, MS analyses identified seven insertions at three distinct splice sites in the C terminus of BKα as well as an extension at the N terminus. At the first site, insertions of either three (IYF, one letter code) or 61 amino acids (termed Strex) (46) were found (corresponding to the alternative usage of exons 22 or 23). At the second site, immediately proximal to a domain termed "Ca^{2+} bowl", an additional stretch of 27 residues encoded by exon 29 (AKPGKLPLVSVNQEKNSGTH-

ILMITEL) was identified. At the C terminus, MS analyses determined four different termini ranging from 8 to 61 residues (resulting from alternative usage of the 3′ part of constitutive exon 33 and the non-constitutive exons 34 and 35 (34)), whereas at the N terminus it was an extension of 65 amino acids resulting from alternative starts of translation. Together, these results verified alternative splicing of BKα at the protein level and determined which splicing events were used in rat brain.

Extensive Phosphorylation of BKα in Rat Brain—Next we investigated the *in vivo* phosphorylation status of BKα by MS analyses of tryptic peptide fragments with and/or without enrichment for phosphopeptides. As illustrated in Figs. 2–4, mass spectrometry identified a total of 30 serine/threonine (Ser/Thr) phosphorylation sites on BKα, 24 of which were found on the constitutive sequence, and six were located on splice extensions. Representative MS/MS spectra of two unique peptides for identified phosphorylation sites Ser(P)-854, Ser(P)-855, Ser(P)-859, and Thr(P)-965 are shown in Fig. 3. Phosphorylated residues at 24 sites were unambiguously assigned based on phosphopeptide MS/MS spectra. Five other sites (Ser(P)-70/Ser(P)-71, Ser(P)-1080/Ser(P)-1082, Ser(P)-1088/Thr(P)-1089 on the constitutive form and Ser(P)-23/Ser(P)-24 within the C-SSP splice insert) were identified where, based on MS/MS spectra of the phosphopeptides, the
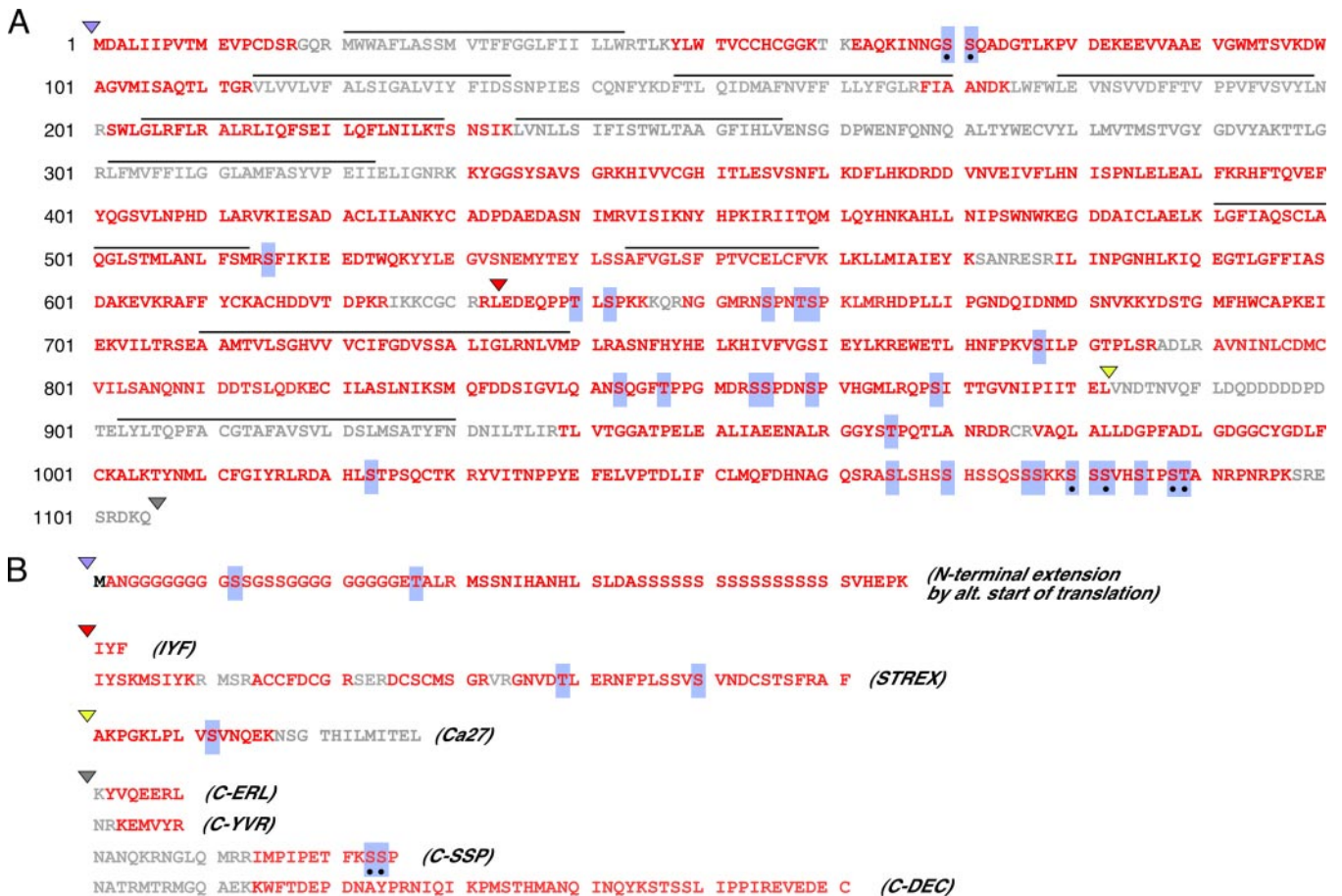
FIG. 2. *In vivo* phosphorylation sites and splice inserts of rat brain BKα identified by MS analysis. *A*, amino acid sequence of the constitutive form of BKα (Swiss-Prot accession number Q62976–2; last 8 residues from splice insert are not included) together with the identified phospho-Ser/Thr residues (highlighted in *blue*) and the splice insertion sites (marked by *colored triangles*). *Dot-free* Ser/Thr residues denote unambiguous phosphorylation sites, whereas *dots* underneath Ser/Thr residues mark ambiguous sites. *B*, amino acid sequence of the identified N-terminal extension and splice variants. Peptides identified by MS analysis are shown in *red*, those not identified in MS analyses are in *gray*. Name of each splice insert is given in bracket on the right side of the amino acid sequence. *Horizontal bars* denote hydrophobic segments S0–S10.

location of the single phosphorylation site within the tryptic peptide could not be unambiguously determined and could be on either of the two neighboring Ser/Thr residues.

Among the 30 identified phosphosites, three were located near the N terminus, Ser(P)-12 and Thr(P)-27 on the N-terminal extension (numbering of these sites refers to their position within the insert itself), and Ser(P)-70/Ser(P)-71 on the intracellular loop between transmembrane segments S0 and S1 (Figs. 2 and 4). All other phosphosites were located on the cytoplasmic C terminus. Site Ser(P)-515 was adjacent to the C-terminal end of S7 close to the RCK1 domain (Fig. 4). Five phosphorylation sites (Thr(P)-640, Ser(P)-642, Ser(P)-655, Thr(P)-658, and Ser(P)-659) were clustered between hydrophobic segments S8 and S9 immediately following the Strex splice site. This region has been suggested to form a flexible linker between the two RCK domains (25, 47). Seven phosphorylation sites were found in the putative RCK2 domain, with Ser(P)-777 located near the C-terminal end of S9, and Ser(P)-843, Thr(P)-847, Ser(P)-854, Ser(P)-855, Ser(P)859,

and Ser(P)-869 clustered near the Ca^{2+}-bowl and the beginning of S10. Another phosphosite detected in the same region was Ser(P)12 on the Ca27 splice insert (Fig. 4). Two sites, Thr(P)-965 and Ser(P)1023 were identified distal to the end of hydrophobic segment S10, whereas another eight phosphorylation sites, including the unambiguous sites Ser(P)-1065, Ser(P)-1070, Ser(P)-1076, Ser(P)-1077, Ser(P)-1081, Ser(P)-1085 and the ambiguous sites at Ser(P)-1080/Ser(P)-1082 and Ser(P)-1088/Thr(P)-1089, were detected at the very C-terminal tail region. The remaining three sites were found on splice inserts: Thr(P)-39 and Ser(P)-50 within the Strex insert and Ser(P)-23/Ser(P)-24 on the C-SSP insert.

The majority of the identified phosphosites were detected on peptides harboring single phosphorylated Ser/Thr residues, whereas the others were found on either doubly phosphorylated peptides (Ser(P)-655, Ser(P)-659, and Ser(P)-843) or triply phosphorylated peptides (Ser(P)-854, Ser(P)-855, Ser(P)-859, Ser(P)-1080, Ser(P)-1082, Ser(P)-1088, and Thr(P)-1089).
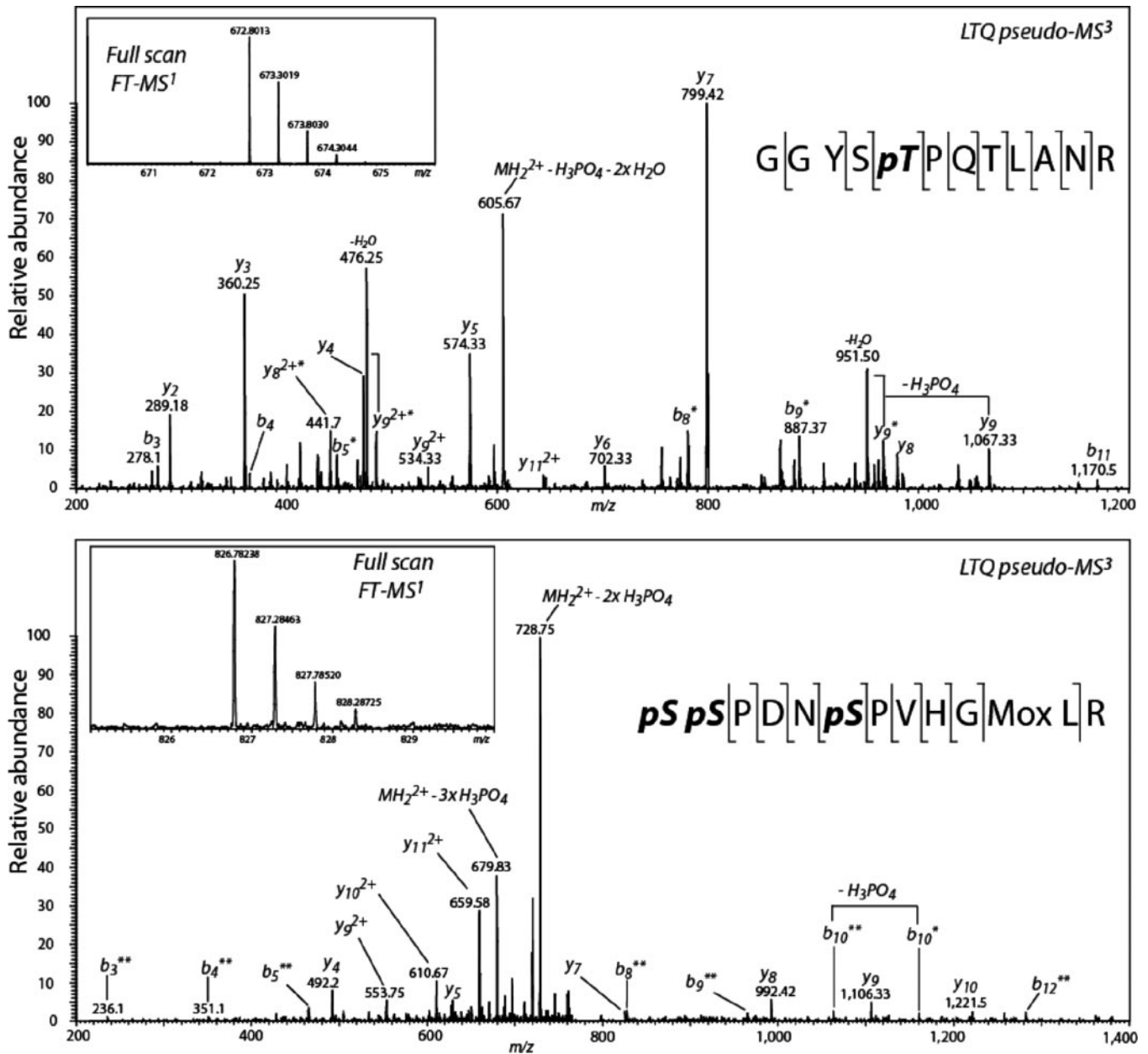
FIG. 3. **Representative MS/MS spectra of two phosphopeptides harboring either one phosphothreonine (Thr(P)-965, *upper panel*) or three phosphoserines (Ser(P)-854/Ser(P)-855/Ser(P)-859, *lower panel*).** Spectra were obtained on an LTQ-Orbitrap mass spectrometer with multistage activation (pseudo-MS3) of the precursor ions shown in the *insets*.

Differential Modulation of BK$_{Ca}$ Channel Gating by Phosphorylation—Next we individually mutated 16 of the identified phospho-Ser/Thr residues on BKα to Ala and Asp attempting to mimic phospho and dephospho states, respectively (48). These mutations were made in the hSlo-HF1 plasmid (45) encoding the constitutive human BKα (accession AAB65837) with the C-terminal splice insert C-ERL; hSlo1 is identical to rat BKα except for five residues (human *versus* rat: A86V, I619V, K631R, S639P, and Q1093P).

Electrophysiological properties of wild type and mutant BK$_{Ca}$ channels were determined in transfected HEK-293 cells

under basal conditions (*i.e.* in the absence of any further stimulus) by patch-clamp recordings in inside-out configuration at different values for [Ca^{2+}]$_i$. Similar to previous studies (45), activation of WT hSlo-HF1 channels was strongly dependent on [Ca^{2+}]$_i$ with half-maximal activation ($V_{1/2}$) occurring at a membrane potential of 149 ± 3 mV (mean ± S.E.) at Ca^{2+}-free conditions ($n = 9$), 97 ± 2 mV at 1.1 μM Ca^{2+} ($n = 11$), 14 ± 2 mV at 10.1 μM Ca^{2+} ($n = 12$), and −35 ± 2 mV at 103 μM Ca^{2+} ($n = 12$; Fig. 5 and Table I). Similar to WT channels, all phosphosite mutants gave rise to robust BK$_{Ca}$ currents, suggesting that none of the phosphosite mutations
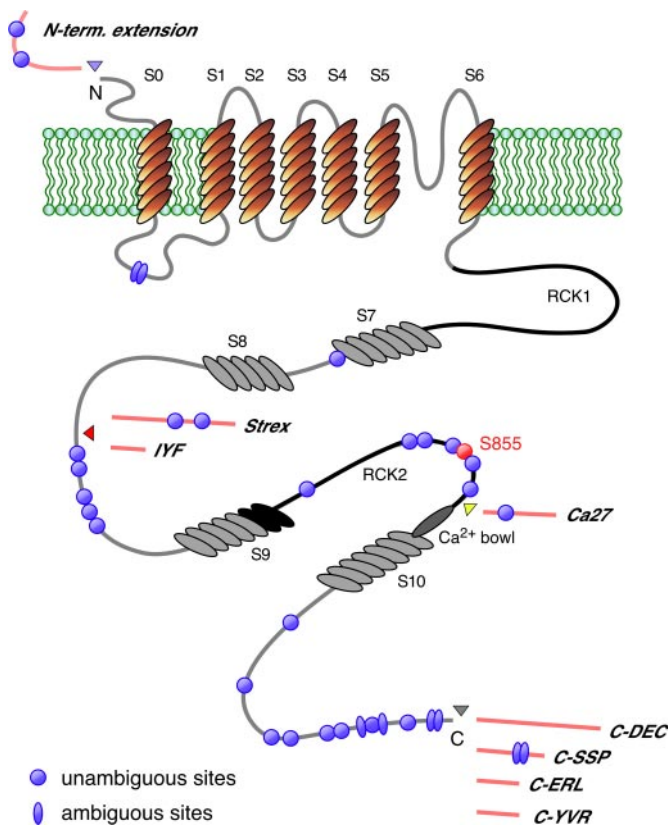
FIG. 4. **Localization of identified phosphosites and splice variants on rat brain BKα.** Membrane topology of BKα together with localization of the identified phosphosites and splice insertions. The constitutive form of BKα contains the transmembrane core (S0–S6), the pore region, the hydrophobic intracellular segments S7–S10, the Ca^{2+} bowl, and the RCK domains (25, 65, 66). Insertion sites of sequence stretches generated by alternative splicing or alternative start of translation are indicated by *triangles* with the same color coding and names as in Fig. 2. Phosphosite Ser(P)-855 exhibiting a marked effect on channel gating is highlighted in *red*.

appreciably affected assembly and trafficking of channels in our heterologous expressions. Alterations in activation gating resulting from introduction of a phosphomimetic negatively charged Asp residue was observed for Ser(P)-855 (Fig. 5*B* and Table I). Compared with the dephospho-mimicking S855A mutant, the $V_{1/2}$ value of S855D displayed a 28 mV shift toward hyperpolarizing potentials, from 152 ± 2 mV ($n = 8$) to 124 ± 3 mV ($n = 9$) under Ca^{2+}-free conditions and of 24 mV, from 102 ± 1 mV ($n = 8$) to 78 ± 2 mV ($n = 9$) at 1.1 μM Ca^{2+}. Smaller shifts (13 and 15 mV) were observed at higher [Ca^{2+}]$_i$ (10.1 and 103 μM, respectively). All other Ala/Asp mutants failed to exert significant changes on channel activation (*i.e.* shifts of $V_{1/2}$ were smaller than 10 mV) (Table I). However, a role of these sites in modulating channel activity in other BKα backbones, or in response to specific signaling events, cannot be excluded. Thus, previous studies on bovine BKα showed that mutating the site corresponding to Ser-869 (identified here as Ser(P)-869) eliminated the 35 mV hyperpolarizing shift in channel activation observed upon treatment of
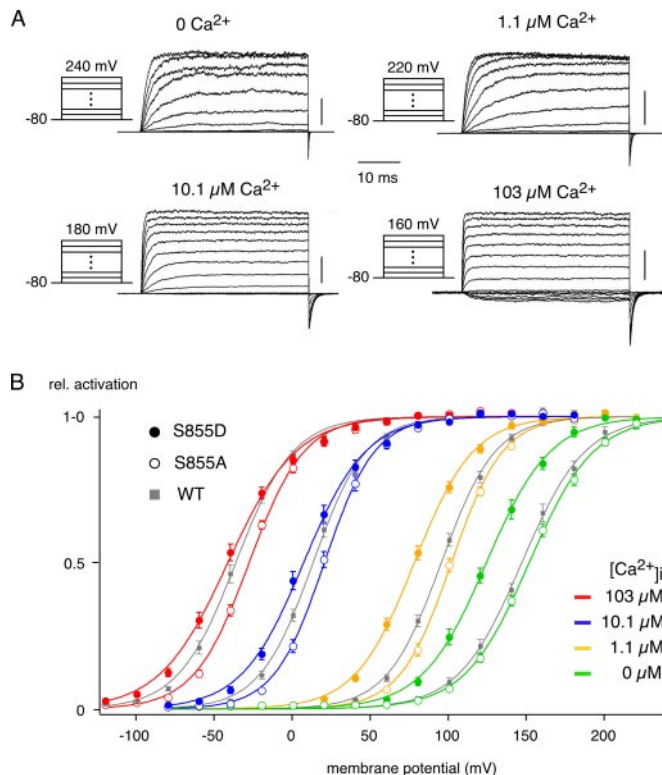

FIG. 5. **Functional characterization of the Ser-855 phosphorylation site.** Macroscopic currents recorded in inside-out patches excised from HEK-293 cells transiently expressing wild type or mutant (S855A and S855D) BK$_{Ca}$ channels. *A,* representative current traces through WT channels recorded at the indicated values for [Ca^{2+}]$_i$, current scaling is 1 nA, time scaling as indicated. *B,* activation curves of WT, S855A, and S855D channels. *Lines* represent fits of single Boltzmann functions to the data points (mean ± S.E., numbers given in Table I).

excised patches with purified PKA (49). Moreover, it should be kept in mind that aspartate mutations may fail to mimic the phosphorylated state because of fundamental differences between the carboxylate anion and the phosphate di-anion and trigonal planar *versus* tetrahedral geometry, respectively (50–53).

DISCUSSION

This work presents the first comprehensive MS analysis on the impact of phosphorylation and alternative splicing of BK$_{Ca}$ channels in rat brain. As central findings, our results identify an unanticipated large number of 30 Ser/Thr residues phosphorylated under *in vivo* conditions and a total of seven splice variations at three distinct sites. Together, these results demonstrate an unexpected level of complexity introduced into the primary structure and properties of BKα by posttranslational modification and alternative splicing.

Analysis of in Vivo Phosphorylation by Mass Spectrometry—For investigation of *in vivo* phosphorylation of the BKα polypeptide, we undertook a proteomic analysis based on a combination of affinity purification of appropriately solubilized

TABLE I

Summary of electrophysiological properties of BKCa WT and phosphorylation site mutants transiently expressed in HEK-293 cells

$V_{1/2}$ is the voltage at half-maximal activation, and z is the equivalent gating charge. Both $V_{1/2}$ and z are obtained by fitting the normalized conductance-voltage relation curve with a single Boltzmann function: $G/G_{max} = 1/(1 + e^{(V_{1/2} - Vm) \ast zF/RT})$. n is number of measured inside-out patches. NA, not available.

Constructs	Ca^{2+}-free			1.1 μM Ca^{2+}			10.1 μM Ca^{2+}			103 μM Ca^{2+}		
	$V_{1/2}$	z	n	$V_{1/2}$	z	n	$V_{1/2}$	z	n	$V_{1/2}$	z	n
	mV			mV			mV			mV		
Wild type	149 ± 3	1.30 ± 0.08	9	97 ± 2	1.51 ± 0.05	11	14 ± 2	1.57 ± 0.05	12	−35 ± 2	1.47 ± 0.04	12
T640A	141 ± 3	1.15 ± 0.12	4	92 ± 5	1.31 ± 0.06	4	9 ± 4	1.37 ± 0.09	5	−43 ± 4	1.20 ± 0.13	5
T640D	144 ± 4	1.12 ± 0.04	6	92 ± 2	1.45 ± 0.05	7	16 ± 3	1.42 ± 0.12	6	−36 ± 2	1.22 ± 0.09	5
S642A	139 ± 1	1.24 ± 0.05	5	85 ± 3	1.59 ± 0.10	7	3 ± 5	1.62 ± 0.15	7	−41 ± 5	1.28 ± 0.10	5
S642D	145 ± 6	1.21 ± 0.09	6	91 ± 5	1.57 ± 0.04	6	7 ± 5	1.60 ± 0.09	6	−40 ± 6	1.33 ± 0.07	6
S655A	153 ± 3	1.13 ± 0.07	4	99 ± 1	1.42 ± 0.08	5	13 ± 3	1.54 ± 0.13	6	−36 ± 1	1.20 ± 0.08	5
S655D	154 ± 6	1.14 ± 0.03	5	97 ± 3	1.63 ± 0.04	7	10 ± 3	1.67 ± 0.05	8	−35 ± 4	1.53 ± 0.04	6
S659A	147 ± 1	1.27 ± 0.16	3	91 ± 3	1.53 ± 0.05	3	5 ± 3	1.52 ± 0.07	5	−36 ± 2	1.57 ± 0.14	3
S659D	140 ± 5	1.32 ± 0.05	4	88 ± 2	1.60 ± 0.09	4	6 ± 2	1.63 ± 0.07	5	−36 ± 2	1.41 ± 0.02	5
S843A	148 ± 5	1.19 ± 0.04	3	100 ± 3	1.62 ± 0.13	6	15 ± 2	1.61 ± 0.12	7	−31 ± 2	1.43 ± 0.08	5
S843D	156 ± 6	1.13 ± 0.06	5	105 ± 3	1.45 ± 0.06	7	25 ± 3	1.49 ± 0.09	7	−25 ± 3	1.25 ± 0.10	7
T847A	153 ± 1	1.16 ± 0.05	5	99 ± 1	1.47 ± 0.03	6	14 ± 1	1.55 ± 0.08	6	−31 ± 2	1.31 ± 0.05	6
T847D	147 ± 5	1.25 ± 0.06	6	97 ± 3	1.52 ± 0.05	6	14 ± 4	1.64 ± 0.13	6	−30 ± 3	1.51 ± 0.12	5
S854A	150 ± 8	1.39 ± 0.02	3	99 ± 3	1.71 ± 0.09	3	13 ± 4	1.70 ± 0.06	3	−37 ± 4	1.38 ± 0.07	3
S854D	152 ± 11	1.36 ± 0.05	3	95 ± 6	1.72 ± 0.11	4	13 ± 5	1.65 ± 0.05	4	−36 ± 7	1.56 ± 0.06	3
S855A	152 ± 2	1.25 ± 0.05	8	102 ± 1	1.59 ± 0.05	8	20 ± 2	1.62 ± 0.06	8	−27 ± 1	1.44 ± 0.09	6
S855D	124 ± 3	1.30 ± 0.07	9	78 ± 2	1.39 ± 0.06	9	7 ± 2	1.36 ± 0.09	10	−42 ± 2	1.22 ± 0.06	9
S859A	153 ± 3	1.22 ± 0.08	6	108 ± 4	1.49 ± 0.11	6	29 ± 4	1.46 ± 0.09	7	−24 ± 2	1.38 ± 0.10	7
S859D	161 ± 3	1.29 ± 0.07	7	115 ± 3	1.43 ± 0.11	7	32 ± 3	1.44 ± 0.08	7	−18 ± 2	1.36 ± 0.11	7
S869A	148 ± 5	1.37 ± 0.13	4	96 ± 4	1.54 ± 0.04	4	10 ± 4	1.71 ± 0.05	4	−38 ± 3	1.59 ± 0.11	4
S869D	148 ± 4	1.45 ± 0.10	6	96 ± 3	1.76 ± 0.06	6	14 ± 3	1.68 ± 0.07	6	−34 ± 4	1.47 ± 0.04	6
T965A	146 ± 2	1.11 ± 0.05	5	94 ± 4	1.27 ± 0.10	5	9 ± 4	1.33 ± 0.10	5	−34 ± 3	1.07 ± 0.05	5
T965D	153 ± 1	1.19 ± 0.04	7	91 ± 3	1.50 ± 0.07	7	4 ± 3	1.44 ± 0.08	6	−40 ± 2	1.19 ± 0.06	6
S1070A	159	1.50	1	101	1.69	1	7 ± 4	1.87 ± 0.05	3	−38 ± 1	1.52 ± 0.10	3
S1070D	155 ± 3	1.23 ± 0.05	3	102 ± 3	1.64 ± 0.12	4	16 ± 3	1.76 ± 0.14	4	−29 ± 3	1.49 ± 0.07	4
S1081A	161 ± 9	1.22 ± 0.10	3	106 ± 6	1.63 ± 0.23	3	20 ± 1	1.73 ± 0.20	3	−30 ± 4	1.44 ± 0.17	3
S1081D	150 ± 1	1.48 ± 0.11	3	101 ± 1	1.78 ± 0.09	3	23 ± 2	1.65 ± 0.11	3	−29 ± 1	1.45 ± 0.07	3
S1082A	144 ± 3	1.27 ± 0.12	3	93 ± 5	1.60 ± 0.13	4	3 ± 2	1.68 ± 0.07	5	−40 ± 3	1.44 ± 0.10	5
S1082D	149 ± 2	1.30 ± 0.09	4	99 ± 2	1.46 ± 0.08	5	7 ± 2	1.71 ± 0.10	7	−30 ± 2	1.42 ± 0.09	6
S1085D	NA	NA		105	1.45	1	12 ± 3	1.76 ± 0.11	5	−29 ± 3	1.55 ± 0.05	4
T1086A	158 ± 1	1.19 ± 0.15	3	102 ± 1	1.69 ± 0.09	3	12 ± 2	1.74 ± 0.02	4	−31 ± 3	1.37 ± 0.09	3
T1086D	159 ± 6	1.11 ± 0.06	3	100 ± 2	1.61 ± 0.12	4	15 ± 4	1.82 ± 0.12	4	−25 ± 4	1.38 ± 0.11	3
S855A/S859A	164 ± 3	1.28 ± 0.06	3	112 ± 5	1.67 ± 0.07	4	33 ± 5	1.67 ± 0.15	5	−20 ± 3	1.48 ± 0.13	4
S855D/S859D	167 ± 5	1.21 ± 0.05	4	120 ± 4	1.49 ± 0.04	4	35 ± 7	1.47 ± 0.13	4	−18 ± 5	1.37 ± 0.10	4
S8-9, 4A	144 ± 5	1.31 ± 0.01	3	105 ± 8	1.41 ± 0.09	3	24 ± 5	1.30 ± 0.02	3	−31 ± 6	1.17 ± 0.05	3
S8-9, 4D	139 ± 6	1.30 ± 0.10	4	91 ± 2	1.48 ± 0.06	4	18 ± 4	1.46 ± 0.13	3	−33 ± 3	1.33 ± 0.06	3
S9-10, 5A	140 ± 2	1.45 ± 0.10	3	85 ± 3	1.64 ± 0.04	3	6 ± 3	1.65 ± 0.04	3	−44 ± 2	1.44 ± 0.06	3
S9-10, 5D	143 ± 4	1.37 ± 0.15	3	100 ± 3	1.35 ± 0.03	3	28 ± 4	1.23 ± 0.01	3	−22 ± 2	1.10 ± 0.13	3

BKα with nano-LC MS/MS analyses (38, 48). Using this approach, we identified a total of 30 Ser/Thr phosphosites, a number that by far exceeds the average number of phosphosites detected in a recent proteomic study on proteins in the soluble fraction of culture cells (41) and even that found for affinity-purified Kv2.1 (48), another ion channel particularly known for its pronounced phospho-regulation (54). In addition both number and pattern of the MS-identified phosphosites markedly differed from the results obtained with computer algorithms, which were widely used in protein/ion channel research and were based on consensus sites of specific protein kinases. As illustrated in Fig. 6, although these algorithms predicted quite a number of phosphosites on the BKα sequence, only a minor subset coincided with the Ser(P)/Thr(P) detected by mass spectrometry on BK$_{Ca}$ channels isolated from native tissue. In other words, in this case prediction

algorithms yielded a significant number of sites that were not phosphorylated under physiological conditions and failed to identify those actually targeted by cellular kinases (Fig. 6B). As further shown in Fig. 6B, the number of "false positives" may be reduced by combining the results of several computer algorithms. However, this strategy comes at the cost of losing many of the *de-facto* phosphorylation sites (Fig. 6B). Taken together the proteomic approach used here appears largely superior in providing comprehensive phospho-analysis of ion channel proteins to conventional (consensus-site based) strategies, although it may still underestimate the actual number of phosphosites present on BKα.

With respect to localization of the identified phosphosites in the BKα primary structure (22), the bulk of identified Ser(P)/Thr(P) are clustered in three regions: the linker region between S8 and S9 near the Strex site, the region close to the Ca^{2+}-
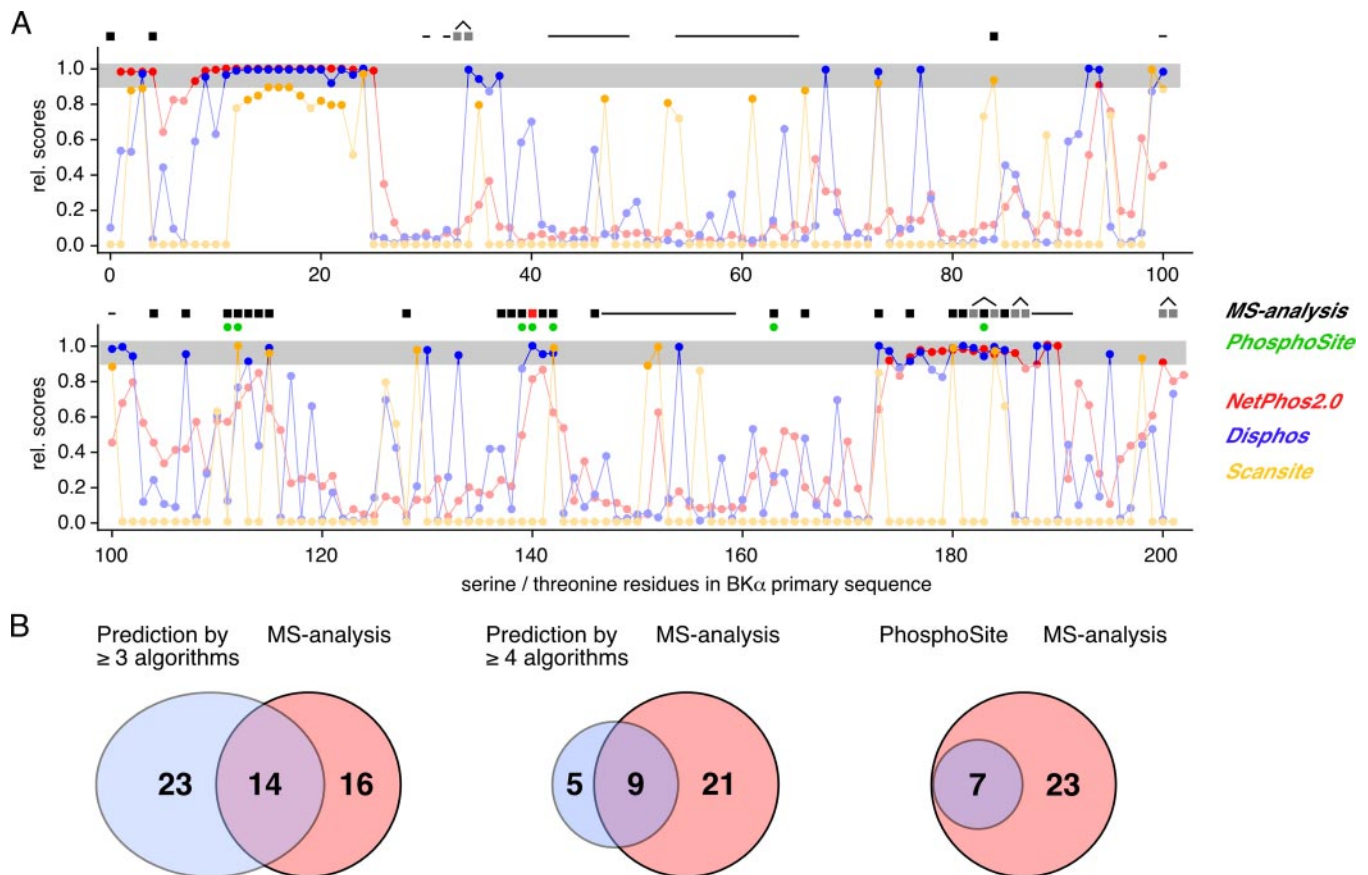
FIG. 6. **Comparison of MS-identified phosphosites on BKα with sites predicted by computer algorithms.** *A*, phosphorylation site predictions for all Ser/Thr residues of BKα (including splice variations) by the indicated algorithms. Scores (given as relative values) considered significant by the individual algorithms are marked by the *gray bar* and by *non-shaded symbols* (for predictions by Scansite). Phosphorylation sites predicted by PhosphoSite are given as filled *green circles*; MS-identified sites are denoted by *black* (unambiguous sites) and *gray rectangles* (ambiguous sites). Ser/Thr residues inaccessible to our MS analyses are marked by *horizontal dashes*. *B*, overlap of phosphosites as predicted by at least three or four computer algorithms (*left* and *middle panel*; for details on the 7 algorithms used see Supplemental Material) or by phosphosite with the 30 sites identified by the MS analyses presented here. Predicted sites are depicted as *blue circles*, identified sites by *red circles*.

bowl and the C-terminal tail (Fig. 4). Two of the identified sites, Ser(P)-869 and Ser(P)-1081, have been previously identified as sites targeted by protein kinases PKA and PKG, respectively (30, 55). The remaining 28 phosphosites represent a *de novo* description. Residues Ser-1098 and Ser-1101 reported as protein kinase C sites (49) could not be verified in our MS analyses because of the low mass of the respective tryptic peptide(s).

The striking extent of BKα phosphorylation raises questions as to its physiological role in regulating neuronal BK$_{Ca}$ channels. Obviously, phosphorylation at some sites is used to modify BK$_{Ca}$ channel gating properties, as demonstrated by the significant $V_{1/2}$ shift observed for certain phospho/dephospho-mimicking mutants, for example S855A/S855D (Fig. 5). Other properties of BK$_{Ca}$ biology regulated through the phosphorylation state may include association with interacting proteins, trafficking to the cell surface, turnover/endocytosis of cell surface channels, targeting to distinct subcellular compartments, etc. (11). The significance of phosphorylation de-

tected for the two residues in the extracellularly located N-terminal extension remains unclear at present.

Analysis of Alternative Splicing by Mass Spectrometry—To date, expression of BKα splice variants has been studied only at the mRNA level (2, 33, 34), and there are only a few reports using mass spectrometry to systematically analyze variants of extensively spliced proteins (56). The high yield of BKα obtained from our affinity purifications allowed for comprehensive MS analysis of splice variations excluding, however, those variants with tryptic fragments too small for mass spectrometry, such as the four residue insert SRKR encoded by the 3'-truncated form of exon 19 or variants providing peptide fragments too low in mass for MS detection. By searching MS/MS spectra of immunopurified BKα against a custom BKα splice variant database, we have identified seven splicing inserts at three different C-terminal sites as well as an N-terminal extension. To our knowledge, this is the first evidence to show that the IYF splice variant and the three C-terminal variants, C-ERL, C-SSP, and C-DEC are present in the mammalian brain.

Alternative inclusion and exclusion of the seven identified splice inserts at three splice sites can form as many as 24 different splicing variants with distinct biophysical properties, or that are altered in other aspects of BK$_{Ca}$ channel biology. For example, expression of Strex-containing BK$_{Ca}$ channels is under hormonal control (46), yielding channels more sensitive to hypoxia (57), and that display a significant hyperpolarizing shift ($\sim$20 mV) in V$_{1/2}$ and considerably slower rates of deactivation when compared with the insertless form (58). The Ca27 splice variant yields channels with an increased activation rate and modified Ca^{2+} cooperativity (59). The C-DEC splice variant generates an extended C terminus resulting in BKα with enhanced retention of newly synthesized BK$_{Ca}$ channels in the endoplasmic reticulum, which finally results in decreased cell surface expression (60, 61). BK$_{Ca}$ channels are robustly expressed in mammalian central neurons (62, 63) and are predominantly localized to axons and presynaptic terminals (17, 37) but are also present in certain neuronal somata and dendrites (18, 64). In rat brain, BKα splice variants may be differentially expressed in distinct cell types or different compartments of the same neuron. A region-specific distribution of the insertless counterpart of Ca27 splice variant has been observed in rat brain, mRNA is predominantly enriched in cerebellum, whereas Ca27 is abundant in all brain regions (59).

REFERENCES

1. Hille, B. (2001) Ionic channels of excitable membranes, 3rd Ed., Sinauer, Sunderland, MA
2. Shipston, M. J. (2001) Alternative splicing of potassium channels: a dynamic switch of cellular excitability. *Trends Cell Biol.* **11,** 353–358
3. Cantrell, A. R., and Catterall, W. A. (2001) Neuromodulation of Na$^+$ channels: an unexpected form of cellular plasticity. *Nat. Rev. Neurosci.* **2,** 397–407
4. Coetzee, W. A., Amarillo, Y., Chiu, J., Chow, A., Lau, D., McCormack, T., Moreno, H., Nadal, M. S., Ozaita, A., Pountney, D., Saganich, M., Vega-Saenz de Miera, E., and Rudy, B. (1999) Molecular diversity of K$^+$ channels. *Ann. N. Y. Acad. Sci.* **868,** 233–285
5. Fury, M., Marx, S. O., and Marks, A. R. (2002) Molecular BKology: the study of splicing and dicing. *Sci STKE* 2002, PE12
6. Gray, A. C., Raingo, J., and Lipscombe, D. (2007) Neuronal calcium channels: splicing for optimal performance. *Cell Calcium* **42,** 409–417
7. Park, K. S., Yang, J. W., Seikel, E., and Trimmer, J. S. (2008) Potassium channel phosphorylation in excitable cells: providing dynamic functional variability to a diverse family of ion channels. *Physiology* **23,** 49–57
8. Schubert, R., and Nelson, M. T. (2001) Protein kinases: tuners of the BKCa channel in smooth muscle. *Trends Pharmacol. Sci.* **22,** 505–512
9. Ghatta, S., Nimmagadda, D., Xu, X., and O'Rourke, S. T. (2006) Large-conductance, calcium-activated potassium channels: structural and functional implications. *Pharmacol. Ther.* **110,** 103–116
10. Gribkoff, V. K., Starrett, J. E., Jr., and Dworetzky, S. I. (2001) Maxi-K potassium channels: form, function, and modulation of a class of endogenous regulators of intracellular calcium. *Neuroscientist* **7,** 166–177
11. Lu, R., Alioua, A., Kumar, Y., Eghbali, M., Stefani, E., and Toro, L. (2006) MaxiK channel partners: physiological impact. *J. Physiol.* **570,** 65–72
12. Salkoff, L., Butler, A., Ferreira, G., Santi, C., and Wei, A. (2006) High-conductance potassium channels of the SLO family. *Nat. Rev. Neurosci.* **7,** 921–931
13. Shao, L. R., Halvorsrud, R., Borg-Graham, L., and Storm, J. F. (1999) The role of BK-type Ca^{2+}-dependent K$^+$ channels in spike broadening during repetitive firing in rat hippocampal pyramidal cells. *J. Physiol.* **521,** 135–146
14. Womack, M. D., and Khodakhah, K. (2002) Characterization of large conductance Ca^{2+}-activated K$^+$ channels in cerebellar Purkinje neurons. *Eur. J. Neurosci.* **16,** 1214–1222
15. Golding, N. L., Jung, H. Y., Mickus, T., and Spruston, N. (1999) Dendritic calcium spike initiation and repolarization are controlled by distinct potassium channel subtypes in CA1 pyramidal neurons. *J. Neurosci.* **19,** 8789–8798
16. Raffaelli, G., Saviane, C., Mohajerani, M. H., Pedarzani, P., and Cherubini, E. (2004) BK potassium channels control transmitter release at CA3-CA3 synapses in the rat hippocampus. *J. Physiol.* **557,** 147–157
17. Hu, H., Shao, L. R., Chavoshy, S., Gu, N., Trieb, M., Behrens, R., Laake, P., Pongs, O., Knaus, H. G., Ottersen, O. P., and Storm, J. F. (2001) Presynaptic Ca^{2+}-activated K$^+$ channels in glutamatergic hippocampal terminals and their role in spike repolarization and regulation of transmitter release. *J. Neurosci.* **21,** 9585–9597
18. Sausbier, U., Sausbier, M., Sailer, C. A., Arntz, C., Knaus, H. G., Neuhuber, W., and Ruth, P. (2006) Ca^{2+}-activated K$^+$ channels of the BK-type in the mouse brain. *Histochem. Cell Biol.* **125,** 725–741
19. Lin, M. T., Hessinger, D. A., Pearce, W. J., and Longo, L. D. (2006) Modulation of BK channel calcium affinity by differential phosphorylation in developing ovine basilar artery myocytes. *Am. J. Physiol. Heart Circ. Physiol.* **291,** H732–H740
20. MacDonald, S. H., Ruth, P., Knaus, H. G., and Shipston, M. J. (2006) Increased large conductance calcium-activated potassium (BK) channel expression accompanied by STREX variant down-regulation in the developing mouse CNS. *BMC Dev. Biol.* **6,** 37
21. Khan, R. N., Smith, S. K., Morrison, J. J., and Ashford, M. L. (1993) Properties of large-conductance K$^+$ channels in human myometrium during pregnancy and labour. *Proc. Biol. Sci.* **251,** 9–15
22. Fodor, A. A., and Aldrich, R. W. (2006) Statistical limits to the identification of ion channel domains by sequence similarity. *J. Gen. Physiol.* **127,** 755–766
23. Jiang, Y., Lee, A., Chen, J., Cadene, M., Chait, B. T., and MacKinnon, R. (2002) Crystal structure and mechanism of a calcium-gated potassium channel. *Nature* **417,** 515–522
24. Jiang, Y., Pico, A., Cadene, M., Chait, B. T., and MacKinnon, R. (2001) Structure of the RCK domain from the *E. coli* K$^+$ channel and demonstration of its presence in the human BK channel. *Neuron* **29,** 593–601
25. Kim, H. J., Lim, H. H., Rho, S. H., Eom, S. H., and Park, C. S. (2006) Hydrophobic interface between two regulators of K$^+$ conductance domains critical for calcium-dependent activation of large conductance Ca^{2+}-activated K$^+$ channels. *J. Biol. Chem.* **281,** 38573–38581
26. Schreiber, M., and Salkoff, L. (1997) A novel calcium-sensing domain in the BK channel. *Biophys. J.* **73,** 1355–1363
27. White, R. E., Schonbrunn, A., and Armstrong, D. L. (1991) Somatostatin stimulates Ca^{2+}-activated K$^+$ channels through protein dephosphorylation. *Nature* **351,** 570–573
28. Reinhart, P. H., Chung, S., Martin, B. L., Brautigan, D. L., and Levitan, I. B. (1991) Modulation of calcium-activated potassium channels from rat brain by protein kinase A and phosphatase 2A. *J. Neurosci.* **11,** 1627–1635
29. White, R. E., Lee, A. B., Shcherbatko, A. D., Lincoln, T. M., Schonbrunn, A.,

and Armstrong, D. L. (1993) Potassium channel stimulation by natriuretic peptides through cGMP-dependent dephosphorylation. *Nature* **361,** 263–266

30. Esguerra, M., Wang, J., Foster, C. D., Adelman, J. P., North, R. A., and Levitan, I. B. (1994) Cloned Ca^{2+}-dependent K$^+$ channel modulated by a functionally associated protein kinase. *Nature* **369,** 563–565

31. Lee, K., Rowe, I. C., and Ashford, M. L. (1995) Characterization of an ATP-modulated large conductance Ca^{2+}-dependent K$^+$ channel present in rat cortical neurons. *J. Physiol. (Lond.)* **488,** 319–337

32. Widmer, H. A., Rowe, I. C., and Shipston, M. J. (2003) Conditional protein phosphorylation regulates BK channel activity in rat cerebellar Purkinje neurons. *J. Physiol.* **552,** 379–391

33. Tseng-Crank, J., Foster, C. D., Krause, J. D., Mertz, R., Godinot, N., DiChiara, T. J., and Reinhart, P. H. (1994) Cloning, expression, and distribution of functionally distinct Ca^{2+}-dependent K$^+$ channel isoforms from human brain. *Neuron* **13,** 1315–1330

34. Beisel, K. W., Rocha-Sanchez, S. M., Ziegenbein, S. J., Morris, K. A., Kai, C., Kawai, J., Carninci, P., Hayashizaki, Y., and Davis, R. L. (2007) Diversity of Ca^{2+}-dependent K$^+$ channel transcripts in inner ear hair cells. *Gene* **386,** 11–23

35. Trimmer, J. S. (1991) Immunological identification and characterization of a delayed rectifier K$^+$ channel polypeptide in rat brain. *Proc. Natl. Acad. Sci. U. S. A.* **88,** 10764–10768

36. Pyott, S. J., Glowatzki, E., Trimmer, J. S., and Aldrich, R. W. (2004) Extrasynaptic localization of inactivating calcium-activated potassium channels in mouse inner hair cells. *J. Neurosci.* **24,** 9469–9474

37. Misonou, H., Menegola, M., Buchwalder, L., Park, E. W., Meredith, A., Rhodes, K. J., Aldrich, R. W., and Trimmer, J. S. (2006) Immunolocalization of the Ca^{2+}-dependent K$^+$ channel Slo1 in axons and nerve terminals of mammalian brain and cultured neurons. *J. Comp. Neurol.* **496,** 289–302

38. Berkefeld, H., Sailer, C. A., Bildl, W., Rohde, V., Thumfart, J. O., Eble, S., Klugbauer, N., Reisinger, E., Bischofberger, J., Oliver, D., Knaus, H. G., Schulte, U., and Fakler, B. (2006) BKCa-Cav channel complexes mediate rapid and localized Ca^{2+}-dependent K$^+$ signaling. *Science* **314,** 615–620

39. Schulte, U., Thumfart, J. O., Klocker, N., Sailer, C. A., Bildl, W., Biniossek, M., Dehn, D., Deller, T., Eble, S., Abbass, K., Wangler, T., Knaus, H. G., and Fakler, B. (2006) The epilepsy-linked Lgi1 protein assembles into presynaptic Kv1 channels and inhibits inactivation by Kvbeta1. *Neuron* **49,** 697–706

40. Pandey, A., Andersen, J. S., and Mann, M. (2000) Use of mass spectrometry to study signaling pathways. *Sci. STKE* **2000,** PL1

41. Olsen, J. V., Blagoev, B., Gnad, F., Macek, B., Kumar, C., Mortensen, P., and Mann, M. (2006) Global, in vivo, and site-specific phosphorylation dynamics in signaling networks. *Cell* **127,** 635–648

42. Thingholm, T. E., Jorgensen, T. J., Jensen, O. N., and Larsen, M. R. (2006) Highly selective enrichment of phosphorylated peptides using titanium dioxide. *Nat. Protoc.* **1,** 1929–1935

43. Olsen, J. V., de Godoy, L. M., Li, G., Macek, B., Mortensen, P., Pesch, R., Makarov, A., Lange, O., Horning, S., and Mann, M. (2005) Parts per million mass accuracy on an Orbitrap mass spectrometer via lock mass injection into a C-trap. *Mol. Cell. Proteomics* **4,** 2010–2021

44. Schroeder, M. J., Shabanowitz, J., Schwartz, J. C., Hunt, D. F., and Coon, J. J. (2004) A neutral loss activation method for improved phosphopeptide sequence analysis by quadrupole ion trap mass spectrometry. *Anal. Chem.* **76,** 3590–3598

45. Meera, P., Wallner, M., Song, M., and Toro, L. (1997) Large conductance voltage- and calcium-dependent K$^+$ channel, a distinct member of voltage-dependent ion channels with seven N-terminal transmembrane segments (S0–S6), an extracellular N terminus, and an intracellular (S9–S10) C terminus. *Proc. Natl. Acad. Sci. U. S. A.* **94,** 14066–14071

46. Xie, J., and McCobb, D. P. (1998) Control of alternative splicing of potassium channels by stress hormones. *Science* **280,** 443–446

47. Qian, X., Niu, X., and Magleby, K. L. (2006) Intra- and intersubunit cooperativity in activation of BK channels by Ca^{2+}. *J. Gen. Physiol.* **128,** 389–404

48. Park, K. S., Mohapatra, D. P., Misonou, H., and Trimmer, J. S. (2006) Graded regulation of the Kv2.1 potassium channel by variable phosphorylation. *Science* **313,** 976–979

49. Zhou, X. B., Arntz, C., Kamm, S., Motejlek, K., Sausbier, U., Wang, G. X., Ruth, P., and Korth, M. (2001) A molecular switch for specific stimulation of the BKCa channel by cGMP and cAMP kinase. *J. Biol. Chem.* **276,** 43239–43245

50. Caillaud, A., Hovanessian, A. G., Levy, D. E., and Marie, I. J. (2005) Regulatory serine residues mediate phosphorylation-dependent and phosphorylation-indepen-dent activation of interferon regulatory factor 7. *J. Biol. Chem.* **280,** 17671–17677

51. Eldar-Finkelman, H., Argast, G. M., Foord, O., Fischer, E. H., and Krebs, E. G. (1996) Expression and characterization of glycogen synthase kinase-3 mutants and their effect on glycogen synthase activity in intact cells. *Proc. Natl. Acad. Sci. U. S. A.* **93,** 10228–10233

52. Gunter, F. (2000) Chemical aspects of peptide bond isomerization. *Chem. Soc. Rev.* **29,** 119–127

53. Shao, J., Prince, T., Hartson, S. D., and Matts, R. L. (2003) Phosphorylation of serine 13 is required for the proper function of the Hsp90 co-chaperone, Cdc37. *J. Biol. Chem.* **278,** 38117–38120

54. Park, K. S., Mohapatra, D. P., and Trimmer, J. S. (2007) Proteomic analyses of Kv2.1 channel phosphorylation sites determining cell background-specific differences in function. *Channels* **1,** 59–61

55. Fukao, M., Mason, H. S., Britton, F. C., Kenyon, J. L., Horowitz, B., and Keef, K. D. (1999) Cyclic GMP-dependent protein kinase activates cloned BKCa channels expressed in mammalian cells by direct phosphorylation at serine 1072. *J. Biol. Chem.* **274,** 10927–10935

56. Paarmann, I., Schmitt, B., Meyer, B., Karas, M., and Betz, H. (2006) Mass spectrometric analysis of glycine receptor-associated gephyrin splice variants. *J. Biol. Chem.* **281,** 34918–34925

57. McCartney, C. E., McClafferty, H., Huibant, J. M., Rowan, E. G., Shipston, M. J., and Rowe, I. C. (2005) A cysteine-rich motif confers hypoxia sensitivity to mammalian large conductance voltage- and Ca^{2+}-activated K$^+$ (BK) channel α subunits. *Proc. Natl. Acad. Sci. U. S. A.* **102,** 17870–17876

58. Chen, L., Tian, L., MacDonald, S. H., McClafferty, H., Hammond, M. S., Huibant, J. M., Ruth, P., Knaus, H. G., and Shipston, M. J. (2005) Functionally diverse complement of large conductance calcium- and voltage-activated potassium channel (BK) α subunits generated from a single site of splicing. *J. Biol. Chem.* **280,** 33599–33609

59. Ha, T. S., Jeong, S. Y., Cho, S. W., Jeon, H., Roh, G. S., Choi, W. S., and Park, C. S. (2000) Functional characteristics of two BKCa channel variants differentially expressed in rat brain tissues. *Eur. J. Biochem.* **267,** 910–918

60. Ma, D., Nakata, T., Zhang, G., Hoshi, T., Li, M., and Shikano, S. (2007) Differential trafficking of carboxyl isoforms of Ca^{2+}-gated (Slo1) potassium channels. *FEBS Lett.* **581,** 1000–1008

61. Kim, E. Y., Ridgway, L. D., Zou, S., Chiu, Y. H., and Dryer, S. E. (2007) Alternatively spliced C-terminal domains regulate the surface expression of large conductance calcium-activated potassium channels. *Neuroscience* **146,** 1652–1661

62. Chang, C. P., Dworetzky, S. I., Wang, J., and Goldstein, M. E. (1997) Differential expression of the α and β subunits of the large-conductance calcium-activated potassium channel: implication for channel diversity. *Brain Res. Mol. Brain Res.* **45,** 33–40

63. Sailer, C. A., Kaufmann, W. A., Kogler, M., Chen, L., Sausbier, U., Ottersen, O. P., Ruth, P., Shipston, M. J., and Knaus, H. G. (2006) Immunolocalization of BK channels in hippocampal pyramidal neurons. *Eur. J. Neurosci.* **24,** 442–454

64. Grunnet, M., and Kaufmann, W. A. (2004) Coassembly of big conductance Ca^{2+}-dependent K$^+$ channels and L-type voltage-gated Ca^{2+} channels in rat brain. *J. Biol. Chem.* **279,** 36445–36453

65. Xia, X. M., Zeng, X., and Lingle, C. J. (2002) Multiple regulatory sites in large-conductance calcium-activated potassium channels. *Nature* **418,** 880–884

66. Yusifov, T., Savalli, N., Gandhi, C. S., Ottolia, M., and Olcese, R. (2008) The RCK2 domain of the human BKCa channel is a calcium sensor. *Proc. Natl. Acad. Sci. U. S. A.* **105,** 376–381